Nonstationary Quasi-perpendicular Shock and Ion Reflection at Mars

Hadi Madanian[1], Steven J. Schwartz[2], Jasper S. Halekas[3], and Lynn Bruce Wilson[4]

[1]Southwest Research Institute
[2]University of Colorado Boulder
[3]University of Iowa
[4]NASA Goddard Space Flight Center

November 21, 2022

Abstract

Collisionless shocks in space plasma are regions of heating and acceleration of charged particles and dissipation of kinetic energy. These accelerated particles are the source of electromagnetic emissions from supernova remnants and other astrophysical structures. At high Mach numbers, shocks can be inherently nonstationary and exhibit modulated energy transfer and recurring plasma compression areas in the form of reformation. We use data from the Mars Atmosphere and Volatile Evolution (MAVEN) spacecraft to study reformation of the Martian bow shock which has a relatively high curvature compared to that at Earth and the upstream solar wind is often mass loaded with a population of pickup ions. We show evidence of ion reflection effects in reformation of a supercritical quasi-perpendicular shock.

1

Nonstationary Quasi-perpendicular Shock and Ion Reflection at Mars

Hadi Madanian[1], Steven J. Schwartz[2], Jasper S. Halekas[3], Lynn B. Wilson III[4]

[1]Southwest Research Institute, San Antonio, TX 78238, United States
[2]Laboratory for Atmospheric and Space Physics, University of Colorado, Boulder, Colorado 80303, United Sates
[3]Department of Physics and Astronomy, University of Iowa, Iowa City, Iowa, 52242 United States
[4]NASA Goddard Space Flight Center, Greenbelt, Maryland, 20771, United States

Key Points:

- Nonstationary bow shock upstream of a nonmagnetized planet
- Reformation of Martian bow shock at high Mach numbers
- Specular reflected solar wind ions and steepended whistler waves upstream of Mars

Corresponding author: Hadi Madanian, `hmadanian@swri.edu`

Abstract

Collisionless shocks in space plasma are regions of heating and acceleration of charged particles and dissipation of kinetic energy. These accelerated particles are the source of electromagnetic emissions from supernova remnants and other astrophysical structures. At high Mach numbers, shocks can be inherently nonstationary and exhibit modulated energy transfer and recurring plasma compression areas in the form of reformation. We use data from the Mars Atmosphere and Volatile Evolution (MAVEN) spacecraft to study reformation of the Martian bow shock which has a relatively high curvature compared to that at Earth and the upstream solar wind is often mass loaded with a population of pickup ions. We show evidence of ion reflection effects in reformation of a supercritical quasi-perpendicular shock.

Plain Language Summary

The interaction of supersonic solar wind with Mars begins at the bow shock, the outer most plasma boundary surrounding the planet. During this interaction, the solar wind flow is slowed down, while incident electrons and ions within the the solar wind are heated to high temperatures. We investigate how the bow shock boundary at Mars at 1.5 Astronomical Units (Astronomical Unit: average Sun-Earth distance) is modified under very high speed solar wind flows.

1 Introduction

In-situ observations of collisionless shocks are limited to laboratory experiments, interplanetary travelling shocks, and planetary bow shocks. In the solar system, the interaction between the supersonic solar wind flow and planetary obstacles that have a global magnetic field or an atmosphere results in the formation of a shock wave upstream of the object. The physical processes within the shock transition layer are nonlinear and vary depending on several characteristic parameters including the Mach number, or the ratio of the flow speed to the relevant wave speed. Above the first critical Mach number, at which the downstream sonic Mach number becomes unity, the shock is considered supercritical. In quasi-perpendicular supercritical shocks, which are emphasized in this letter, the angle between the upstream magnetic field and the local normal vector to the shock surface (θ_{bn}) is greater than $45°$, and they exhibit a well-defined and clear transition that includes a foot, ramp, and overshoot (Burgess & Scholer, 2015; Leroy et al., 1982). At quasi-parallel shocks ($\theta_{bn} < 45°$) upstream particle dynamics, trajectories, and turbulence are very different (Shan et al., 2020).

Energy conversion at collisionless shocks can occur through coupling between electromagnetic instabilities and charged particles (Kennel et al., 2013; Coroniti, 1970). These instabilities are mostly driven by electric currents generated in or near the relatively thin ramp layer. With increasing Mach number, other dissipative and dispersive mechanisms take effect, which operate at different length and time scales. Some of the energy is transported by emission of dispersive whistler waves, a branch of magnetosonic waves generated at the shock front, to the upstream (Tidman & Northrop, 1968; Russell, 2007). Supercritical shocks also dissipate energy by reflecting solar wind ions. The reflected ions experience the upstream motional electric field which accelerates and returns these ions to the bow shock. The spatial extent of the reflected ion trajectory marks the foot region of the shock, which typically shows a gradual increase in the magnetic field upstream of the steep main shock ramp (Bale et al., 2005).

Highly supercritical shocks can be inherently nonstationry and in some cases reform. Numerical simulations have shown that accumulation of specular (or nearly specular) reflected ions upstream of high Mach number shocks can lead to quasi-periodic enhancements in the magnetic field and cyclic reformation of the shock front, with a pe-

riod in the order of the upstream ion gyroperiod (Biskamp & Welter, 1972; Lembege & Savoini, 1992; Hada, 2003). Other theoretical studies have suggested that nonstationarity and reformation are entirely based on steepening of dispersive whistler waves, and the shock front ramp itself is a high amplitude steepened nonlinear whistler wave (Krasnoselskikh et al., 2002, 2013; Galeev et al., 1988). In these studies, dispersion effects are dominant while effects due to other micro instabilities are not included. Models of whistler-induced reformation (Scholer & Burgess, 2007), and reformation due to modified two-stream instability (Scholer & Matsukiyo, 2004) have also been proposed.

The fundamental physical processes of reformation in collisionless shocks are poorly understood and are far from being settled, in part due to limited in-situ measurements of the processes. A few studies have shown evidence of nonstationarity and reformation at the terrestrial (Dimmock et al., 2019; Lobzin et al., 2007; Sundberg et al., 2017; Lefebvre et al., 2009; Mazelle et al., 2010), and planetary bow shocks (Shan et al., 2020; Sulaiman et al., 2015; Tiu et al., 2011). Nonstationarity can also manifest itself in the form of shock ripples formed near the shock overshoot (Johlander et al., 2016). Most of these studies cover shock phenomena upstream of planets with large scale magnetic dipoles and bow shock boundaries. Nonstationarity and the dynamics of collisionless shocks in environments containing an abundance of pickup ions, and where the ion gyroradius is comparable to the length scales of the system have rarely been discussed.

Mars lacks a global magnetic dipole; nonetheless, a bow shock and an induced magnetosphere are present (Bertucci et al., 2011). In this letter, we investigate nonstationarity of the Martian bow shock which has a relatively high curvature compared to the terrestrial and outer planetary counterparts. The population of pickup ions from the extended neutral corona upstream of Mars can be significant, which can change the characteristics of the bow shock.

2 Observations

We study a quasi-perpendicular supercritical bow shock crossing event at Mars on 15 August 2016 using MAVEN data (Jakosky et al., 2015). The magnetic field data are from the Magnetometer sensor which measures the magnetic field with up to 32 Hz sampling rate (Connerney et al., 2015). The ion data are from the Solar Wind Ion Analyzer (SWIA) instrument (Halekas et al., 2015) which measures ions in the 25 eV – 25 keV en-

Table 1. Upstream plasma and shock parameters

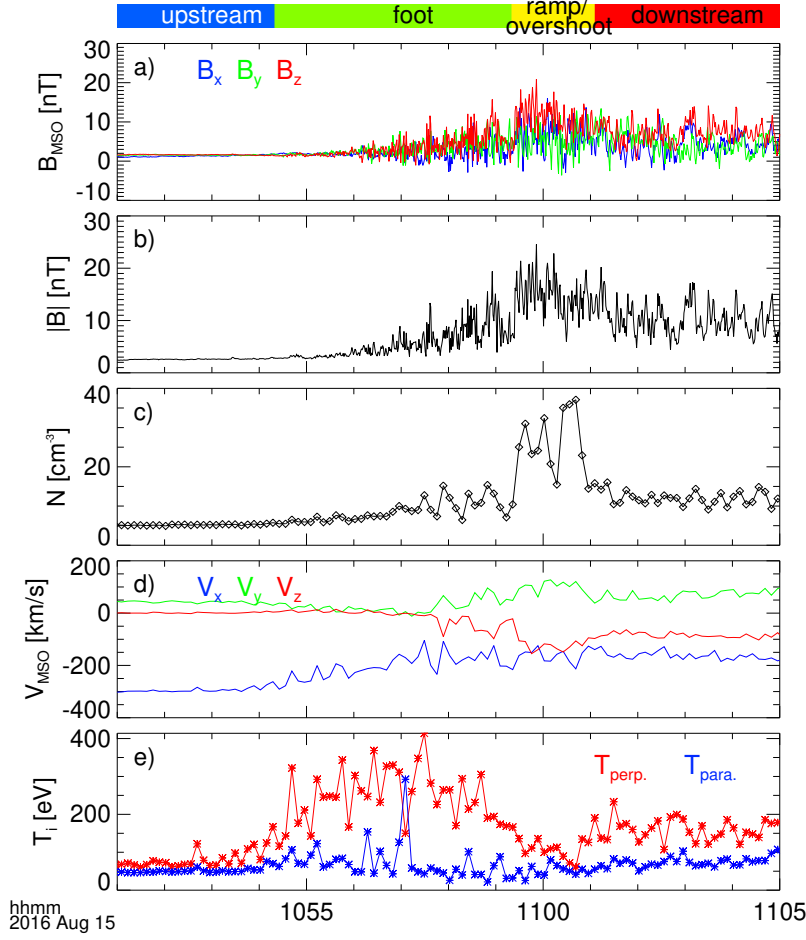| Parameter	Value
$|\mathbf{B}_{up}|$ IMF Magnitude (nT)	2.6
Solar wind density (cm^{-3})	5.4
$|\mathbf{V}_{up}|$ Solar wind speed (kms^{-1})	325
β_{Ion}	1.5
Proton gyroperiod (s)	24.2
Thermal proton gyroradius (km)	118
Convected proton gyroradius (km)	1200
M_A Alfvénic Mach number	12.2
M_{MS} Magnetosonic Mach number	6.4
$\hat{\mathbf{n}}$ (MSO)	(0.85, 0.3, -0.4)
θ_{Bn}	72
θ_{Vn}	34
$V_{shock-\hat{\mathbf{n}}}$ (kms^{-1})	5

Figure 1. Overview of the shock crossing event on 15 August 2016. (a) Magnetic field components in the Mars-centered Solar Orbital (MSO) coordinates in which $+x$ is toward the Sun and $+z$ is normal to the orbital plane, (b) magnetic field magnitude, (c) plasma density, (d) bulk plasma flow velocity components, and (e) ion temperatures in the local magnetic field frame. Different regions of the shock are labeled in the top colorbar. The spacecraft speed is about 2.8 kms^{-1} with respect to Mars. R_M: Mars radius $\sim$ 3390 km.

63 ergy range with a 22.5° angular resolution over a total field of view of 2.8π solid angle
64 every 8 s. The ion moments are calculated in a similar way as in Madanian et al. (2019);
65 Halekas et al. (2017).

66   The Alfvénic and fast magnetosonic Mach numbers are about 12.2 and 6.4, respec-
67 tively, which place this shock in the highly supercritical regime. Other solar wind and
68 shock parameters are listed in Table 1. An overview of plasma, and magnetic field data
69 during this crossing event is shown in Figure 1. Panels (a) and (b) show the magnetic
70 field components and magnitude at 1 Hz sampling rate. The orbit segment of the shown
71 data begins in the pristine solar wind at 10:51:00 UTC from (1.5, 0.5, -0.9) R_M, and ends
72 inside the magnetosheath at 11:05:00 UTC at (0.8, 0.8, -1.0) R_M.

73   The yellow segment in the top colorbar marks the main shock layer, which includes
74 the ramp and overshoot. The shock ramp at 10:59:30 UTC is characterized by a sharp
75 increase in the magnetic field strength along with a jump in the plasma density. Mag-
76 netic field fluctuations immediately downstream of the ramp reach the highest level, and
77 the plasma is highly compressed with compression ratios much greater than the predicted
78 values by Rankine-Hugoniot relations. This region of extra compression is followed by
79 a short asymptotic decrease to downstream sheath values. Since the spacecraft is near
80 the ramp, these variations could be interpreted as shock ripples. However, a tell-tale sig-
81 nature of shock ripples, which we do not observe here, is when the transverse compo-
82 nent of the local magnetic field oscillates across ripples due to a non-planar shock front
83 (Johlander et al., 2016).

84   In the foot region the magnetic field profile shows pulse-like enhancements, peri-
85 odically accumulated in bunches that are correlated with underlying plasma density in-
86 creases. The pulsations are sharp, and the maximum amplification ratio within each group
87 reaches levels comparable to the downstream magnetic field, suggestive of a nonstation-
88 ary shock behaviour. Upstream of the shock front, the bulk plasma velocity shows some
89 variability, while ion temperatures shown in panel (e) are highly anisotropic. As will be
90 further demonstrated in the next section, this temperature anisotropy is associated with
91 solar wind ions reflected from the shock and driven by the motional electric field $\mathbf{E}_{up} =$
92 $-\mathbf{V}_{up} \times \mathbf{B}_{up}$. The perpendicular ion temperature is in fact modulated by multiple beams
93 of reflected ions.

2.1 Ion Reflection and Dynamics

95   Figure 2 shows a close-up view of nonstationarity features in the foot region. Panel
96 (a) shows the magnetic field profile and panel (b) shows the non-solar wind ion densi-
97 ties. To subtract the solar wind contribution we use and interpolate data from the SWIA
98 fine mode designed to track and measure solar wind beam ions at a particular subset of
99 energies and directions (Halekas et al., 2015). Quasi-periodic enhancements in the mag-
100 netic field and ion density are seen in panels (a) and (b), with an average period of $\sim$
101 30 s, comparable to the upstream proton gyroperiod 24.2 s. Similar periodic modula-
102 tions have been observed upstream of Earth and Saturn which were attributed to the
103 reformation of the bow shock at high Mach numbers (Sundberg et al., 2017; Sulaiman
104 et al., 2015).

105   We analyze ion populations around these structure in more detail. To distinguish
106 reflection in ion data we use the normal incidence frame (NIF) (Schwartz, 1998). The
107 NIF frame transformation velocity is obtained from $\mathbf{V}_{NIF} = \hat{\mathbf{n}} \times (\mathbf{V}_{up} \times \hat{\mathbf{n}})$, where $\hat{\mathbf{n}}$
108 is the shock normal vector and $\mathbf{V}_{up}$ is the upstream solar wind velocity in the shock rest
109 frame (i.e., after subtracting the shock velocity along $\hat{\mathbf{n}}$). We use a bow shock bound-
110 ary model (Trotignon et al., 2006) to calculate $\hat{\mathbf{n}}$. Given the large amplitude magnetic
111 field fluctuations downstream of the shock, the co-planarity method (Schwartz, 1998) and
112 methods that rely on fields and or velocity vectors in the downstream are unreliable for
113 determining the shock orientation. Based on the time to traverse the shock foot, we es-
114 timate the shock speed along the normal direction to be $V_{shock-\hat{\mathbf{n}}} \sim$5 kms^{-1} (Gosling
115 & Thomsen, 1985), which is much smaller than the normal component of the solar wind
116 flow. We have neglected this small correction to $\mathbf{V}_{up}$ in our analysis. We also show the
117 data in shock-normal coordinates ($\hat{\mathbf{n}}$, $\hat{\mathbf{t}}_1$, $\hat{\mathbf{t}}_2$) in which $\hat{\mathbf{t}}_2 = \hat{\mathbf{n}} \times \hat{\mathbf{B}}_{up}$ and $\hat{\mathbf{t}}_1$ completes
118 the right-hand system. In the NIF frame, the $\hat{\mathbf{t}}_2$ axis is approximately along $\mathbf{E}_{up}$ and
119 $\hat{\mathbf{t}}_1$ is parallel to the component of $\mathbf{B}_{up}$ that is tangent to the shock surface.

120   A spectrogram of ion phase space densities as a function of V_n is shown in Figure
121 2.c. Reflected ions with $+V_n$ and varying intensities are observed upstream of the shock,
122 indicating a modulated ion reflection process in the foot. Panels (d-i) show 2D cuts through
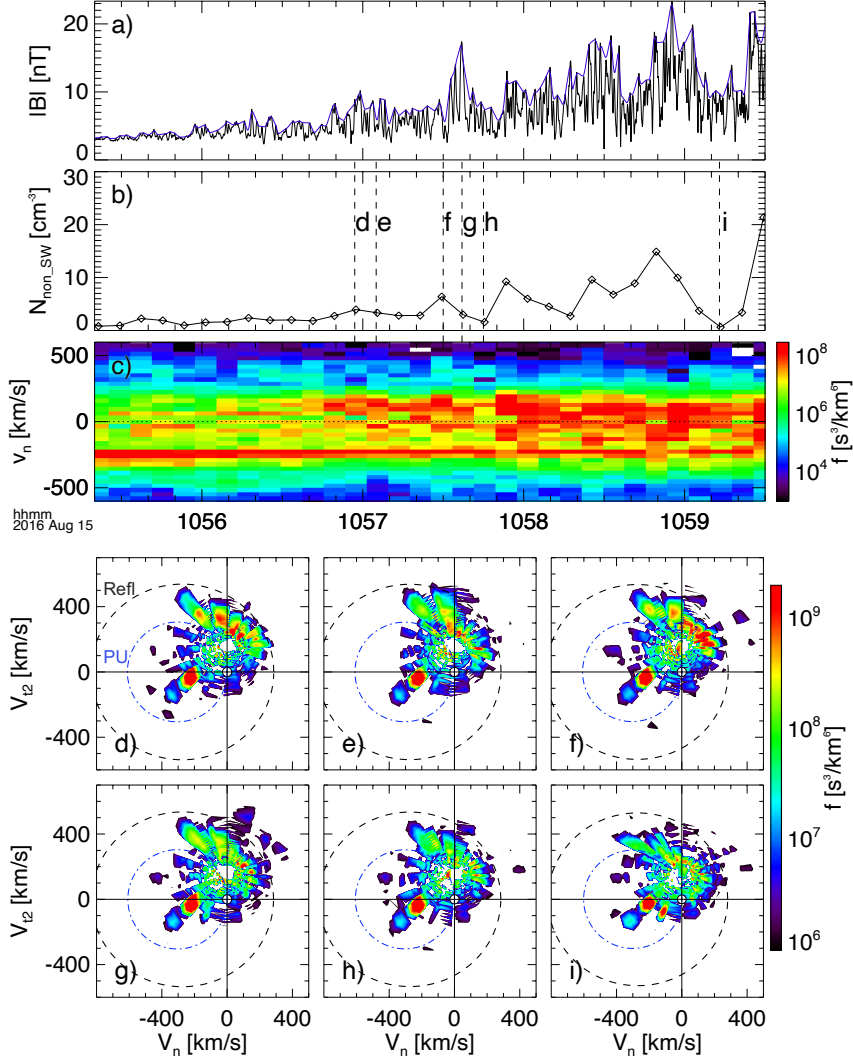123 the ion phase space distributions as a function of V_n and V_{t2} around two consecutive en-

Figure 2. Ion reflection upstream of the shock. (a) Magnetic field profile (black) and its maximum signal envelope (blue), (b) non-solar wind ion densities, (c) ion phase space density spectrogram as a function of V_n averaged over V_{t1} and V_{t2}, (d-i) 2D cuts through ion phase space densities in the $\hat{\mathbf{n}} - \hat{\mathbf{t}}_2$ plane averaged over V_{t1}. The black ellipses and blue circles are the predicted trajectories of specularly reflected ions ("Refl") and hydrogen pickup ions ("PU"), respectively.

124 hancement cycles. Corresponding timestamps are marked in panel (b). The dashed el-
125 lipses on these panels show the predicted velocity track of the reflected ions. Specularly
126 reflected ions in the solar wind rest frame have speeds of $2|\mathbf{V}_{up}.\hat{\mathbf{n}}|$, which is different than
127 the relative speed of pickup hydrogen ions (blue circles).

128   The distribution in (d) is measured at the fifth density peak from the shock. In ad-
129 dition to the solar wind beam around $V_n \sim -250$ to -300 kms^{-1}, the distribution shows
130 ions with $+V_n$ velocities that extend to zero and then $-V_n$ following along the black el-
131 lipse. These are reflected ions at different gyrophases as they travel away from and back
132 toward the shock. The magnetic field also shows a modest enhancement at this time. The
133 distribution in panel (e) is downstream of (d) where the reflected ion density has decreased
134 and the decreasing trend continues until the next cycle begins. The high intensity ion

population in (f) is associated with the next peak in the density time series, and is followed by less intense flux of reflected ions in panels (g-h). An isolated low amplitude peak in the magnetic field is observed near timestamp (f); however, much higher amplitude perturbations are measured few seconds later around distribution (g) when the plasma density has decreased. We also observe in panels (d-h) signatures of pickup ions ($V_n \sim -50$, $V_{t2} \sim 150$ kms^{-1}) along the blue circles. The distribution in panel (i) is closest to the shock and similarly, shows reflected and returning ions, some of which have gained $|-V_n|$ velocities higher than the incident solar wind. Near the shock, the solar wind is slowed down and incident ions undergoing reflection have speeds lower than the pristine solar wind, $|V| < |\mathbf{V}_{up} \cdot \hat{\mathbf{n}}|$, which could explain why reflected ions are often inside the dashed ellipse. The reflection may also be non-specular (Sundberg et al., 2017).

Data presented in Figure 2 indicate that upstream density enhancements are caused by reflected ions. Correlated with density enhancements, we observe increased magnetic field strength and perturbations. The nonstationary nature of this shock crossing, and the characteristic periodicity observed in upstream enhancements are consistent with a reforming bow shock.

2.2 Whistler Waves and Source of Reformation

Whistler waves are commonly observed upstream of shocks. These waves are intrinsically right-hand circularly polarized but can be observed as left-handed if Doppler-shifted by the motion of the plasma over the spacecraft (Wilson et al., 2012, 2017). Wave activities around the reformation cycles discussed in Figure 2 show whistler type signatures. Figures 3.(a) and (b) show the the smoothed (using a 0.25 s sliding window) magnetic field magnitude and components around the fourth reformation sequence. In panel (c) we show background subtracted magnetic field vectors in the minimum variance coordinates for two intervals when whistler waves are observed. Both waves are circular and minimum variance analyses are well conditioned. The ratios of the transformation matrix eigenvalues (λ_1 maximum, λ_2 intermediate, and λ_3 minimum) for the wave packet near 10:57:20 UTC are $\lambda_1/\lambda_2 \sim 1.7$ and $\lambda_2/\lambda_3 \sim 10.1$, and the second wave packet near 10:57:35 UTC shows $\lambda_1/\lambda_2 \sim 1.6$ and $\lambda_2/\lambda_3 \sim 24.8$.

The hodograms of the second wave packet are shown in panels (d-f). Variation in panel (d) is clockwise, and the direction of wave propagation is into the page. Since the background field (B_{bkg}) points out of the page, the wave is left-handed. The wave frequency in the spacecraft frame is ~ 0.4 Hz. Previous statistical studies have identified these waves as whistler type (Brain, 2002). In the interval shown, each whistler wave packet lasts only a few seconds. Since the shock is reforming, during a part of the reformation cycle, the shock could emit nonlinear whistlers that can escape into the upstream, but not during other parts of the cycle. Therefore, in the upstream one could observe intermittent whistler pulses. The waves are Doppler shifted and must be moving towards the shock.

When the amplitude of a whistler wave becomes large enough, the electric field of the wave can cause ion reflection (Krasnoselskikh et al., 2013; Comişel et al., 2011). For the second whistler wave packet shown in Figure 3.c, the highest amplitude of the fluctuations, corresponding to the maximum electric field that would reflect ions, is at 10:57:37 UTC, downstream of and after the peak ion reflection is observed (the bracket in panel (a)).

We identify three possible scenarios to describe these observations with respect to the reformation process:

- Reflected ions are from a downstream reflection point (i.e., the previous reformation sequence) and create a new shock during the reformation process. Whistler
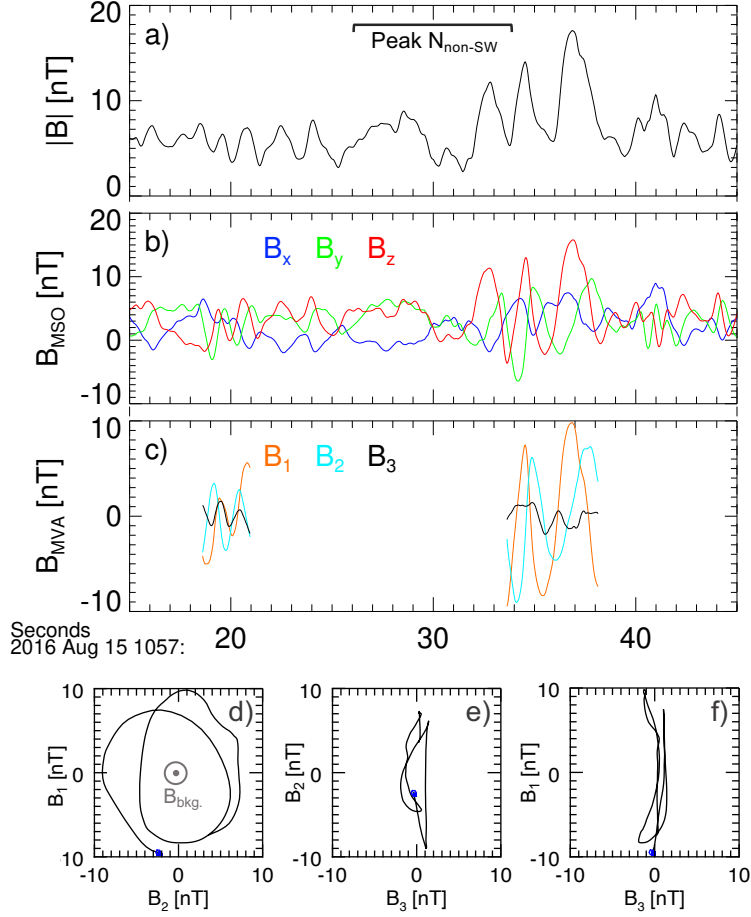
Figure 3. Whistler wave signatures. (a) Magnetic field strength, (b) magnetic field components in MSO coordinates, (c) background subtracted magnetic field transformed into minimum variance coordinates. Panels (d-f) show the hodograms of the minimum variance components of the second wave packet. The blue dots mark the begining of the interval. The 8 s timestamp bracket of the closest ion density peak (distribution (f) in Figure 2) is specified on panel (a).

waves are generated at the new shock and later pass by the spacecraft as they are carried towards the main shock by the solar wind.

- Reflected ions interact locally with Doppler shifted whistler waves in the foot and cause steepening in the waves, similar to the process described in Scholer and Burgess (2007).
- Reflected ions create only a modest enhancement in $|B|$, as seen in Figure 3.a between the wave packets, but this effect is independent of the high amplitude waves.

Lack of information about the motion of waves and reflection surfaces relative to the spacecraft, and unknown point of generation of waves complicate accurate identification of the order of events during reformation. It is however, unlikely that the reformation cycles discussed here are purely caused by steepened whistler waves, but rather ion reflection appears to be a significant driving mechanism. This may be a result of the moderate upstream plasma β.

3 Conclusions

In this letter, we report on nonstationarity of a supercritical quasi-perpendicular shock at Mars. In the foot region of the shock, we observe quasi-periodic pulsations and enhancements in magnetic field and ion density which can be explained by the shock reformation process. We show that ion density enhancements are due to reflected ions. The density peaks are accompanied by increased magnetic field strength and elevated levels of magnetic turbulence. Interaction of reflected ions and the incident solar wind can result in a variety of locally generated turbulence, which can coincide with and modulate the magnetic field variations caused by the reformation cycles. This is in addition to whistler waves generated by the shock waves. The cyclic enhancements have a characteristic period of ~ 30 s, or 1.2 times the upstream solar wind proton gyroperiod, which agrees with simulations and previous observations of shock reformation (Lembege & Savoini, 1992; Hada, 2003; Sulaiman et al., 2015). Recurring enhancements observed downstream of the shock in the magnetosheath are also consistent with old reformation structures.

These results illustrate shock reformation in the unique plasma environment of Mars that has characteristic length scales much different than the Earth. The solar wind ion convective gyroradius at Mars is larger than the size of the magnetosheath. The reflected ion gyroradius is also large and ions may return to a bow shock location which could have different conditions (e.g., θ_{bn}, shock potential, wave activities) than their initial reflection point. This aspect could have an influence on the whole reflection process and the shock dynamics, since the fields within the ramp should be maintained self-consistently. Future modeling studies which include full kinetic effects and realistic ion to electron mass ratios are needed to capture more details of the shock reformation process and its possible impacts on Mars.

References

Bale, S. D., Balikhin, M. A., Horbury, T. S., Krasnoselskikh, V. V., Kucharek, H., Möbius, E., . . . Thomsen, M. F. (2005, June). Quasi-perpendicular Shock Structure and Processes. *Space Science Reviews*, *118*(1-4), 161–203. doi: 10.1007/s11214-005-3827-0

Bertucci, C., Duru, F., Edberg, N., Fraenz, M., Martinecz, C., Szego, K., & Vaisberg, O. (2011, December). The Induced Magnetospheres of Mars, Venus, and Titan. *Space Science Reviews*, *162*(1-4), 113–171. doi: 10.1007/s11214-011-9845-1

Biskamp, D., & Welter, H. (1972, December). Numerical studies of magnetosonic collisionless shock waves. *Nuclear Fusion*, *12*(6), 663–666. doi: 10.1088/0029-5515/12/6/006

Brain, D. A. (2002). Observations of low-frequency electromagnetic plasma waves upstream from the Martian shock. *Journal of Geophysical Research*, *107*(A6). doi: 10.1029/2000JA000416

Burgess, D., & Scholer, M. (2015). *Collisionless Shocks in Space Plasmas: Structure and Accelerated Particles*. Cambridge: Cambridge University Press. doi: 10.1017/CBO9781139044097

Comişel, H., Scholer, M., Soucek, J., & Matsukiyo, S. (2011, February). Non-stationarity of the quasi-perpendicular bow shock: comparison between Cluster observations and simulations. *Annales Geophysicae*, *29*(2), 263–274. doi:

10.5194/angeo-29-263-2011

Connerney, J. E. P., Espley, J., Lawton, P., Murphy, S., Odom, J., Oliversen, R., & Sheppard, D. (2015, December). The MAVEN Magnetic Field Investigation. *Space Science Reviews*, *195*(1-4), 257–291. doi: 10.1007/s11214-015-0169-4

Coroniti, F. V. (1970, May). Dissipation discontinuities in hydromagnetic shock waves. *Journal of Plasma Physics*, *4*(2), 265–282. doi: 10.1017/S0022377800004992

Dimmock, A. P., Russell, C. T., Sagdeev, R. Z., Krasnoselskikh, V., Walker, S. N., Carr, C., . . . Balikhin, M. A. (2019, February). Direct evidence of nonstationary collisionless shocks in space plasmas. *Science Advances*, *5*(2), eaau9926. doi: 10.1126/sciadv.aau9926

Galeev, A. A., Gringauz, K. I., Klimov, S. I., Remizov, A. P., Sagdeev, R. Z., Savin, S. P., . . . Schwingenschuh, K. (1988). Physical processes in the vicinity of the cometopause interpreted on the basis of plasma, magnetic field, and plasma wave data measured on board the Vega 2 spacecraft. *Journal of Geophysical Research*, *93*(A7), 7527. doi: 10.1029/JA093iA07p07527

Gosling, J. T., & Thomsen, M. F. (1985). Specularly reflected ions, shock foot thicknesses, and shock velocity determinations in space. *Journal of Geophysical Research*, *90*(A10), 9893. doi: 10.1029/JA090iA10p09893

Hada, T. (2003). Shock front nonstationarity of supercritical perpendicular shocks. *Journal of Geophysical Research*, *108*(A6). doi: 10.1029/2002JA009339

Halekas, J. S., Brain, D. A., Luhmann, J. G., DiBraccio, G. A., Ruhunusiri, S., Harada, Y., . . . Jakosky, B. M. (2017, November). Flows, Fields, and Forces in the Mars-Solar Wind Interaction: Mars-Solar Wind Interaction. *Journal of Geophysical Research: Space Physics*, *122*(11), 11,320–11,341. doi: 10.1002/2017JA024772

Halekas, J. S., Taylor, E. R., Dalton, G., Johnson, G., Curtis, D. W., McFadden, J. P., . . . Jakosky, B. M. (2015, December). The Solar Wind Ion Analyzer for MAVEN. *Space Science Reviews*, *195*(1-4), 125–151. doi: 10.1007/s11214-013-0029-z

Jakosky, B. M., Lin, R. P., Grebowsky, J. M., Luhmann, J. G., Mitchell, D. F., Beutelschies, G., . . . Zurek, R. (2015, December). The Mars Atmosphere and Volatile Evolution (MAVEN) Mission. *Space Science Reviews*, *195*(1-4), 3–48. doi: 10.1007/s11214-015-0139-x

Johlander, A., Schwartz, S., Vaivads, A., Khotyaintsev, Y. V., Gingell, I., Peng, I., . . . Burch, J. (2016, October). Rippled Quasiperpendicular Shock Observed by the Magnetospheric Multiscale Spacecraft. *Physical Review Letters*, *117*(16). doi: 10.1103/PhysRevLett.117.165101

Kennel, C. F., Edmiston, J. P., & Hada, T. (2013, March). A Quarter Century of Collisionless Shock Research. In R. G. Stone & B. T. Tsurutani (Eds.), *Geophysical Monograph Series* (pp. 1–36). Washington, D. C.: American Geophysical Union. doi: 10.1029/GM034p0001

Krasnoselskikh, V., Balikhin, M., Walker, S. N., Schwartz, S., Sundkvist, D., Lobzin, V., . . . Comisel, H. (2013, October). The Dynamic Quasiperpendicular Shock: Cluster Discoveries. *Space Science Reviews*, *178*(2-4), 535–598. doi: 10.1007/s11214-013-9972-y

Krasnoselskikh, V., Lembège, B., Savoini, P., & Lobzin, V. V. (2002, April). Nonstationarity of strong collisionless quasiperpendicular shocks: Theory and full particle numerical simulations. *Physics of Plasmas*, *9*(4), 1192–1209. doi: 10.1063/1.1457465

Lefebvre, B., Seki, Y., Schwartz, S. J., Mazelle, C., & Lucek, E. A. (2009, November). Reformation of an oblique shock observed by Cluster: REFORMATION OF AN OBLIQUE SHOCK. *Journal of Geophysical Research: Space Physics*, *114*(A11), A11107. doi: 10.1029/2009JA014268

Lembege, B., & Savoini, P. (1992, November). Nonstationarity of a two-dimensional

quasiperpendicular supercritical collisionless shock by self-reformation. *Physics of Fluids B: Plasma Physics*, *4*(11), 3533–3548. doi: 10.1063/1.860361

Leroy, M. M., Winske, D., Goodrich, C. C., Wu, C. S., & Papadopoulos, K. (1982, July). The structure of perpendicular bow shocks. *Journal of Geophysical Research: Space Physics*, *87*(A7), 5081–5094. doi: 10.1029/JA087iA07p05081

Lobzin, V. V., Krasnoselskikh, V. V., Bosqued, J.-M., Pinçon, J.-L., Schwartz, S. J., & Dunlop, M. (2007, March). Nonstationarity and reformation of high-Mach-number quasiperpendicular shocks: Cluster observations: SHOCK FRONT REFORMATION. *Geophysical Research Letters*, *34*(5). doi: 10.1029/2006GL029095

Madanian, H., Halekas, J., Mazelle, C., Omidi, N., Espley, J., Mitchell, D., & Mc-Fadden, J. (2019, December). Magnetic Holes Upstream of the Martian Bow Shock: MAVEN Observations. *Journal of Geophysical Research: Space Physics*. doi: 10.1029/2019JA027198

Mazelle, C., Lembège, B., Morgenthaler, A., Meziane, K., Horbury, T. S., Génot, V., . . . Pantellini, F. (2010). Self-Reformation of the Quasi-Perpendicular Shock: CLUSTER Observations. In (pp. 471–474). Saint-Malo, (France). doi: 10.1063/1.3395905

Russell, C. (2007, October). Upstream whistler-mode waves at planetary bow shocks: A brief review. *Journal of Atmospheric and Solar-Terrestrial Physics*, *69*(14), 1739–1746. doi: 10.1016/j.jastp.2006.11.004

Scholer, M., & Burgess, D. (2007, July). Whistler waves, core ion heating, and non-stationarity in oblique collisionless shocks. *Physics of Plasmas*, *14*(7), 072103. doi: 10.1063/1.2748391

Scholer, M., & Matsukiyo, S. (2004, July). Nonstationarity of quasi-perpendicular shocks: a comparison of full particle simulations with different ion to electron mass ratio. *Annales Geophysicae*, *22*(7), 2345–2353. doi: 10.5194/angeo-22-2345-2004

Schwartz, S. J. (1998). Shock and Discontinuity Normals, Mach Numbers, and Related Parameters. In G. Paschmann & P. W. Daly (Eds.), *Analysis Methods for Multi-Spacecraft Data (ISSI Scientific Reports Series)* (Vol. 1, pp. 249–270).

Shan, L., Du, A., Tsurutani, B. T., Ge, Y. S., Lu, Q., Mazelle, C., . . . Henri, P. (2020, January). In Situ Observations of the Formation of Periodic Collisionless Plasma Shocks from Fast Mode Waves. *The Astrophysical Journal*, *888*(2), L17. doi: 10.3847/2041-8213/ab5db3

Sulaiman, A., Masters, A., Dougherty, M., Burgess, D., Fujimoto, M., & Hospodarsky, G. (2015, September). Quasiperpendicular High Mach Number Shocks. *Physical Review Letters*, *115*(12). doi: 10.1103/PhysRevLett.115.125001

Sundberg, T., Burgess, D., Scholer, M., Masters, A., & Sulaiman, A. H. (2017, February). The Dynamics of Very High Alfvén Mach Number Shocks in Space Plasmas. *The Astrophysical Journal*, *836*(1), L4. doi: 10.3847/2041-8213/836/1/L4

Tidman, D. A., & Northrop, T. G. (1968, March). Emission of plasma waves by the Earth's bow shock. *Journal of Geophysical Research*, *73*(5), 1543–1553. doi: 10.1029/JA073i005p01543

Tiu, D., Cairns, I. H., Yuan, X., & Robinson, P. A. (2011, April). Evidence for reformation of the Uranian bow shock: Hybrid simulations and comparisons with Voyager data: EVIDENCE OF SHOCK REFORMATION. *Journal of Geophysical Research: Space Physics*, *116*(A4), A04228. doi: 10.1029/2010JA016057

Trotignon, J., Mazelle, C., Bertucci, C., & Acuña, M. (2006, April). Martian shock and magnetic pile-up boundary positions and shapes determined from the Phobos 2 and Mars Global Surveyor data sets. *Planetary and Space Science*, *54*(4), 357–369. doi: 10.1016/j.pss.2006.01.003

Wilson, L. B., Koval, A., Szabo, A., Breneman, A., Cattell, C. A., Goetz, K., . . . Pulupa, M. (2012, April). Observations of electromagnetic whistler precursors at supercritical interplanetary shocks: WHISTLER PRECURSORS-PARTICLES. *Geophysical Research Letters*, *39*(8), L08109. doi: 10.1029/2012GL051581

Wilson, L. B., Koval, A., Szabo, A., Stevens, M. L., Kasper, J. C., Cattell, C. A., & Krasnoselskikh, V. V. (2017, September). Revisiting the structure of low-Mach number, low-beta, quasi-perpendicular shocks: SHOCK STRUCTURE. *Journal of Geophysical Research: Space Physics*, *122*(9), 9115–9133. doi: 10.1002/2017JA024352